

## An Analysis of Cutting and Machining Using Fracture Mechanics Concepts

J. G. Williams<sup>\*1,2</sup>, Y. Patel<sup>1</sup> and B.R.K. Blackman<sup>1</sup>

<sup>1</sup> Mechanical Engineering Department, Imperial College London, London SW7 2AZ, UK.

<sup>2</sup> Aero, Mechanical and Mechatronics Engineering Department, University of Sydney, Australia.

\*g.williams@imperial.ac.uk

**Keywords:** Machining, fracture mechanics, fracture toughness, adhesion toughness, root rotation, elastic bending, elastic-plastic bending, work hardening, polymers, metals.

**Abstract.** The process of cutting and machining is analysed using concepts developed in the fracture analysis of beam specimens. Increasing loads and decreasing tool rake angles lead to a sequence of deformation processes from elastic bending, elastic-plastic bending and finally shear yielding in the chip. The conditions for each mode to occur are identified. Fracture toughness is included in the analysis as is, in addition, the notion of root rotation at the crack tip. This gives rise to the tool touching at the crack tip under some circumstances during which energy is transferred directly to the fracture process. The tool-chip interface is characterised by Coulomb friction and an adhesion toughness. Experimental data for polymers and metals taken from the literature is analysed. Values of fracture and adhesion toughness are deduced as well as yield stress and friction coefficients. There is evidence of work hardening and also that the root rotation affects the angle of the shear plane. Chip curling is also discussed.

### Introduction

The analysis of machining processes has a long history [e.g. 1-3] with several reviews available [e.g. 4]. The motivation was to improve machine tools and the analysis focussed on describing friction effects and the plastic deformation of chip formation [5-7]. The latter was the subject of considerable effort using slip line theory and attempts were made to resolve the various solutions via experimental studies [8].

The issue of whether fracture and cracks played any part in the process has a complex history. This was proposed by Reuleaux in 1900 [9] but subsequently abandoned because the energies were, erroneously, said to be too small. In addition, the absence of visible cracks was thought to be important. Atkins has firmly established that these omissions were wrong and that the fracture terms are important in any cutting analysis [10, 11].

The similarity of cutting a layer from a surface and splitting a cantilever specimen with a wedge has been observed previously [12] and it is therefore possible to take analyses developed for double cantilever beam specimens and apply them to cutting. This includes the notion of root rotation at the crack tip and plasticity in the arms [13].

In this work, these ideas are explored in greater detail and are extended to include the case of when the tool tip touches the crack tip. The inclusion of shear yielding in the beam (chip) and the issue of chip curling are also addressed.

Figure 1 shows the three stages of the deformation as the load is increased and/or the rake angle of the tool is decreased. In Figure 1(a) the deformation is elastic, apart from a thin layer of plastic deformation on the inner chip surface and cut surface of the workpiece. In such cases the chips are straight, apart from a small amount of inward curvature arising from the plasticity on the chip. In Figure 1(b) the loads have increased sufficiently to involve plastic bending in the arm which creates chip curling, though some curvature is recovered elastically. The ‘crack tip touching’ condition is reached when the tool tip reaches the crack tip. This is also shown in Figure 1(b). In Figure 1(c) a

further increase in load or decrease in rake angle induces a shear deformation in the chip along a slip plane as well as bending. Under these circumstances the crack tip touching condition is more easily achieved.

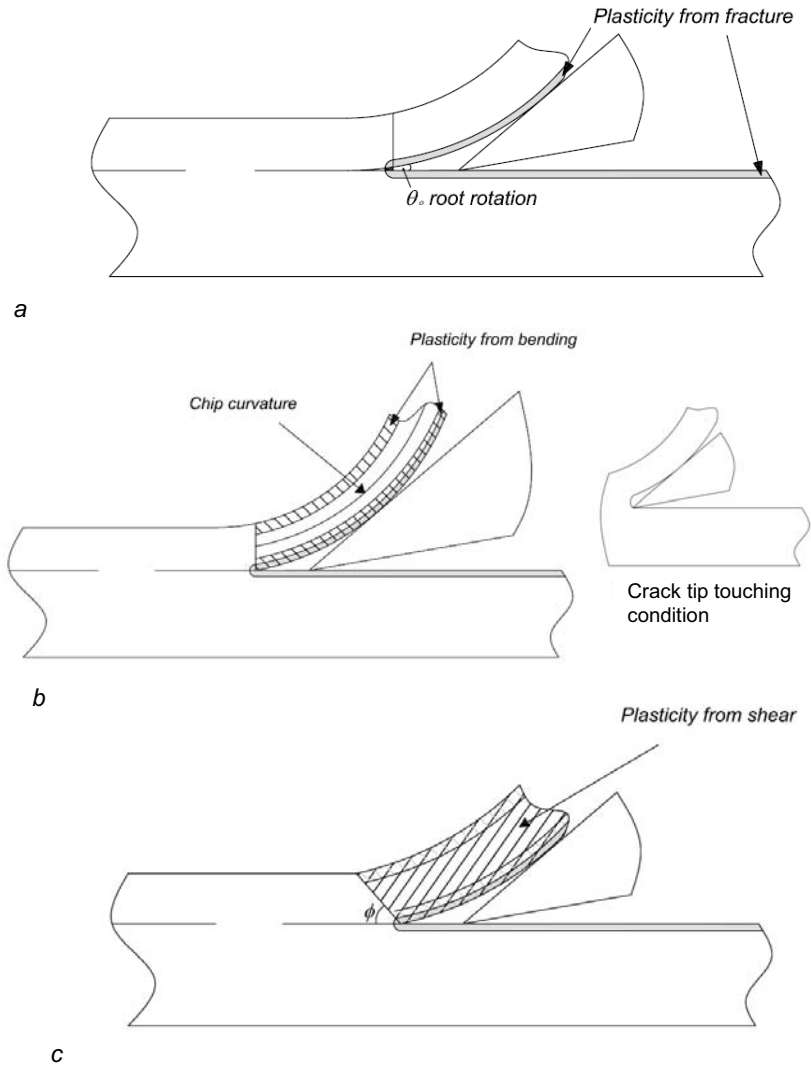


Figure 1: Three stages of deformation: (a) Elastic; (b) Plastic bending and (c) Shear.



$$\frac{S}{b} = \frac{F_c}{b} \sin \alpha + \frac{F_t}{b} \cos \alpha$$

and

$$(2.3)$$

$$\frac{N}{b} = \frac{F_c}{b} \cos \alpha - \frac{F_t}{b} \sin \alpha$$

$$\frac{S}{b} = \mu \frac{N}{b} + G_a$$

$$(2.4)$$

where  $\mu$  is the coefficient of friction between the tool and the chip. On substituting into equation (2.3) gives:

$$\frac{F_t}{b} = Z \frac{F_c}{b} + \frac{G_a}{\cos \alpha + \mu \sin \alpha}$$

$$(2.5)$$

where

$$Z = \frac{\mu - \tan \alpha}{1 + \mu \tan \alpha} = \tan(\beta - \alpha) \text{ where } \mu = \tan \beta$$

Steady state fracture problems such as this can often be solved by an equilibrium approach or via energy. This analysis starts using the former and deduces the bending moment,  $M$ , at a general point  $B$  where the surface slope is  $\psi$ , as shown in Figure 2:

$$\frac{M}{b} = \frac{F_c}{b} \left( v_0 - \left( v + \frac{h}{2} \cos \psi \right) \right) - \frac{F_t}{b} \left( x + \frac{h}{2} \sin \psi \right)$$

and

$$(2.6)$$

$$\frac{d}{d\psi} \left( \frac{M}{b} \right) = \frac{F_c}{b} \left( -\frac{dv}{d\psi} + \frac{h}{2} \sin \psi \right) - \frac{F_t}{b} \left( \frac{dx}{d\psi} + \frac{h}{2} \cos \psi \right)$$

Now

$$\frac{dx}{d\psi} = - \left( R + \frac{h}{2} \right) \cos \psi$$

$$(2.7a)$$

$$\frac{dv}{d\psi} = \left( R + \frac{h}{2} \right) \sin \psi$$

$$(2.7b)$$

and

$$\frac{dv}{dx} = - \tan \psi$$

$$(2.7c)$$

For elastic bending,

$$\frac{1}{R} = \frac{12}{Eh^3} \left( \frac{M}{b} \right) \text{ and } \frac{d}{d\psi} \left( \frac{M}{b} \right) = - \frac{Eh^3}{12} \frac{1}{R^2} \frac{dR}{d\psi}$$

$$(2.8)$$

and on substituting equations (2.7) and (2.8) in equation (2.6) gives

$$\frac{Eh^3}{12} \frac{1}{R^3} \frac{dR}{d\psi} = \frac{F_c}{b} \sin \psi - \frac{F_t}{b} \cos \psi$$

This may be integrated and noting that  $R \rightarrow \infty$  at  $\psi = \frac{\pi}{2} - \alpha$  we have,

$$\frac{Eh^3}{24} \frac{1}{R^2} = \frac{F_c}{b} (\cos \psi - \sin \alpha) + \frac{F_t}{b} (\sin \psi - \cos \alpha) \quad (2.9)$$

At  $\psi = \theta_0 \ll 1$ ,  $R = R_0$  and so,

$$\frac{Eh^3}{24} \frac{1}{R_0^2} = \frac{F_c}{b} (1 - \sin \alpha) + \frac{F_t}{b} (\theta_0 - \cos \alpha).$$

The energy release rate at  $\theta$  due to bending is given by,

$$G_b = \frac{6}{Eh^3} \left( \frac{M_0}{b} \right)^2 = \frac{Eh^3}{24} \frac{1}{R_0^2}$$

and there is a contribution from  $\frac{F_t}{b}$  acting at  $\theta$  which is given by:

$$G_t = \frac{F_t}{b} \frac{dv}{dx} = -\frac{F_t}{b} \theta_0$$

and hence the total energy release rate is expressed in equation (2.10),

$$G = G_b + G_t = \frac{Eh^3}{24} \frac{1}{R_0^2} - \frac{F_t}{b} \theta_0 = \frac{F_c}{b} (1 - \sin \alpha) - \frac{F_t}{b} \cos \alpha \quad (2.10)$$

and on substituting from equation (2.5)

$$G = \frac{F_c}{b} \left( 1 - \frac{\mu}{\cos \alpha + \mu \sin \alpha} \right) - \frac{G_a \cos \alpha}{\cos \alpha + \mu \sin \alpha} \quad (2.11)$$

It is noteworthy that since there is no change in elastic energy, then for  $\mu = 0$ , and  $G_a = 0$ ,  $\frac{F_c}{b} = G$

i.e. there is no dissipation. For finite  $\mu$  and  $G_a$  then  $\frac{F_c}{b} > G$ .

This result may be obtained rather more simply via energy. For a steady state in which the crack and the load move forward by  $dx$  then the increment of external work is,

$$d \left( \frac{U_{ext}}{b} \right) = \frac{F_c}{b} dx$$

The dissipated energy is,

$$\left( d \frac{U_d}{b} \right) = \frac{S}{b} dx = \left[ \mu \left( \frac{F_c}{b} \cos \alpha - \frac{F_t}{b} \right) + G_a \right] dx$$

and on substituting for  $\frac{F_t}{b}$  from equation (2.5) gives

$$d \left( \frac{U_d}{b} \right) = \left[ \frac{F_c}{b} \frac{\mu}{\cos \alpha + \mu \sin \alpha} + \frac{G_a \cos \alpha}{\cos \alpha + \mu \sin \alpha} \right] dx$$

Now

$$G dx = d \left( \frac{U_{ext}}{b} \right) - d \left( \frac{U_d}{b} \right)$$

which gives equation (2.11).

It should be noted that for cutting a material in which  $G = G_c$  the cutting force, from equation (2.11), becomes

$$\frac{F_c}{b} = \left( \frac{1}{1 - \mu \left( \frac{1 - \sin \alpha}{\cos \alpha} \right)} \right) \left[ G_c (1 + \mu \tan \alpha) + G_a \right] \quad (2.12)$$

i.e.  $\frac{F_c}{b}$  is independent of  $h$  but a function of both  $\mu$  and  $G_a$  as expected.

If  $\frac{F_t}{b}$  is also measured then, from equation (2.5),  $\mu$  and  $G_a$  may be found and then  $G_c$  determined from equation (2.12).

### Crack Tip Touching

Another aspect of the proposed model is the inclusion of crack tip rotation and displacement, permitting the tool tip to reach point  $\theta$  as the force is increased. As the force is increased further there would be a reaction on the tool but  $R_\theta$  would thereafter remain the same. The crack tip touching condition is shown schematically in Figure 1(b) and may be expressed, using equation 2.7 as:

$$\Delta + v_o \tan \alpha = \int_0^{\frac{\pi}{2} - \alpha} \left( R + \frac{h}{2} \right) \cos \psi \, d\psi$$

from equation 2.7(a) and

$$v_o = \int_0^{\frac{\pi}{2} - \alpha} \left( R + \frac{h}{2} \right) \sin \psi \, d\psi$$

from equation 2.7(b). Therefore,

$$\chi h = \frac{h}{2}(f_1) + \frac{1}{\cos \alpha} \int_0^{\frac{\pi}{2}-\alpha} R \cos(\psi + \alpha) d\psi$$

where

$$f_1 = \frac{1 - \sin \alpha}{\cos \alpha}$$

Here we may use equation (2.9) to find  $R$  as a function of  $\psi$ . The general case with friction and  $G_a$  is rather complicated for this large displacement solution but a useful result may be found by using the  $\mu = G_a = 0$  case for which  $\frac{F_t}{b} = -\frac{F_c}{b} \tan \alpha$ . Thus equation (2.9) becomes,

$$\left(\frac{R_0}{R}\right)^2 = \frac{\cos(\psi + \alpha)}{\cos \alpha}$$

and hence

$$\left(\frac{h}{2R_0}\right) (2\chi - (f_1)) = \frac{1}{\sqrt{\cos \alpha}} \int_0^{\frac{\pi}{2}-\alpha} \sqrt{\cos(\psi + \alpha)} d\psi = f_2 \quad (3.1)$$

where  $f_2$  must be evaluated numerically.

The root rotation angle at this condition is given by:

$$\sin \bar{\theta}_{02} = \frac{\chi h}{R_0 + \frac{h}{2}} = \frac{2\chi f_2}{(f_2 - f_1) + 2\chi} \quad (3.2)$$

where  $\bar{\theta}$  implies crack tip touching and the subscripts 02 represents the elastic, frictionless conditions. A further useful solution is obtained by assuming that  $R$  remains constant at  $R_0$  and in this case equation (3.1) becomes,

$$\left(\frac{h}{2R_0}\right) (2\chi - f_1) = f_1 \quad (3.3)$$

and

$$\sin \bar{\theta}_{01} = f_1 \quad (3.4)$$

where subscript 01 denotes this constant  $R$  condition at  $R_0$ .

Table :1 Crack tip touching functions

$\alpha$ (°)	$f_1 = \sin \bar{\theta}_{01}$	$f_2 = \sin \bar{\theta}_{02}$	
-20	>1	-	>1
-10	>1	-	>1
0	1.00	-	>1
10	0.84	1.03	0.90
20	0.70	0.88	0.77
30	0.58	0.74	0.66
40	0.47	0.60	0.55
50	0.36	0.47	0.43
60	0.27	0.35	0.33
70	0.18	0.23	0.22
80	0.09	0.12	0.11
90	0	0	0

Table 1 shows values of  $f_1, f_2, \bar{\theta}_{01}$ , and  $\bar{\theta}_{02}$  for the practical range of  $\alpha$  values and there is only about 20% difference in the results for the two assumptions. Clearly the solutions have no meaning for small  $\alpha$  values since  $\sin \bar{\theta}_0 > 1$  and indeed  $\left(\frac{h}{2R_0}\right)$  must be  $< 0.15$  to have any significance because of the limitations of beam theory, i.e. a strain of 15%. These touching solutions are thus only likely to occur for  $\alpha > 70^\circ$  and a simple approximation for the condition would be,

$$\sin \bar{\theta}_0 = \bar{\theta}_0 = f_1 \text{ and } \frac{h}{2R_0} = \frac{\bar{\theta}_0}{2\chi} \quad (3.5)$$

If touching does occur then there would be a force per unit width,  $G_e$ , acting on the tool tip which goes directly into  $G$  from equations (2.17), i.e.

$$G = G_b + G_t + G_e \quad (3.6)$$

with

$$G_b = \bar{G}_b = \frac{Eh}{6} \left(\frac{h}{2R_0}\right)^2 = \frac{Eh}{24\chi^2} \bar{\theta}_0^2$$

and

$$G_t = -\frac{F_t}{b} \bar{\theta}_0$$

Equation (2.10) for  $G$  is also modified in that  $\frac{F_c}{b}$  becomes  $\left(\frac{F_c}{b} - G_e\right)$  and similarly in equation (2.5) to give,

$$G = \frac{F_c}{b} \left( 1 - \frac{\mu}{\cos \alpha + \mu \sin \alpha} \right) - \frac{G_a \cos \alpha}{\cos \alpha + \mu \sin \alpha} + \frac{\mu G_e}{\cos \alpha + \mu \sin \alpha} \quad (3.7)$$

The same expression may be derived by the energy route but a solution can only be found if  $G_e$  can be determined. From equation (3.6)

$$G_e = G - \bar{G}_b + \frac{F_1}{b} \bar{\theta}_0$$

and from equation (2.5)

$$\frac{F_c}{b} = Z \left( \frac{F_c}{b} - G_e \right) + \frac{G_a}{\cos \alpha + \mu \sin \alpha}$$

and hence

$$G_e = \frac{1}{1 + Z\bar{\theta}_0} \left[ G - \bar{G}_b + Z\bar{\theta}_0 \frac{F_c}{b} + \frac{\bar{\theta}_0 G_a}{\cos \alpha + \mu \sin \alpha} \right]$$

and on substituting into equation (3.7) we have,

$$G = \frac{F_c}{b} - \frac{G_a}{\cos \alpha + \mu \sin \alpha} \left( \frac{\cos \alpha (1 + Z\bar{\theta}_0) - \frac{\mu \bar{\theta}_0}{\cos \alpha + \mu \sin \alpha}}{(1 + Z\bar{\theta}_0) - \frac{\mu}{\cos \alpha + \mu \sin \alpha}} \right) - \frac{1}{(\cos \alpha + \mu \sin \alpha) (1 + Z\bar{\theta}_0) - \frac{\mu}{\cos \alpha + \mu \sin \alpha}} \frac{\mu E h}{24 \chi^2} \bar{\theta}_0^2 \quad (3.8)$$

The approximate touching condition is given by equation (3.5), i.e.

$$\bar{\theta}_0 = \frac{1 - \sin \alpha}{\cos \alpha}$$

and hence,

$$1 + Z\bar{\theta}_0 = \frac{(1 - \sin \alpha) + \mu \cos \alpha}{\cos \alpha (\cos \alpha + \mu \sin \alpha)}$$

and on substituting into equation (3.8) we have the rather surprisingly simple result:

$$G = \frac{F_c}{b} - G_a - \frac{\mu E h}{24 \chi^2} \left( \frac{1 - \sin \alpha}{\cos \alpha} \right)$$

For tests on materials with a fixed  $G = G_c$  value  $\frac{F_c}{b}$  now has a linear dependence on  $h$ , thus:

$$\frac{F_c}{b} = G_c + G_a + \frac{\mu E}{24\chi^2} \left( \frac{1 - \sin \alpha}{\cos \alpha} \right) h \quad (3.9)$$

This is shown schematically in Figure 3, together with the non touching case, expressed by equation (2.12). The transition between the two conditions occurs at the thickness  $\hat{h}$  given by:

$$\hat{h} = \frac{24\chi^2}{E} \left( G_a + \frac{G_c}{1 - \sin \alpha} \right) \quad (3.10)$$

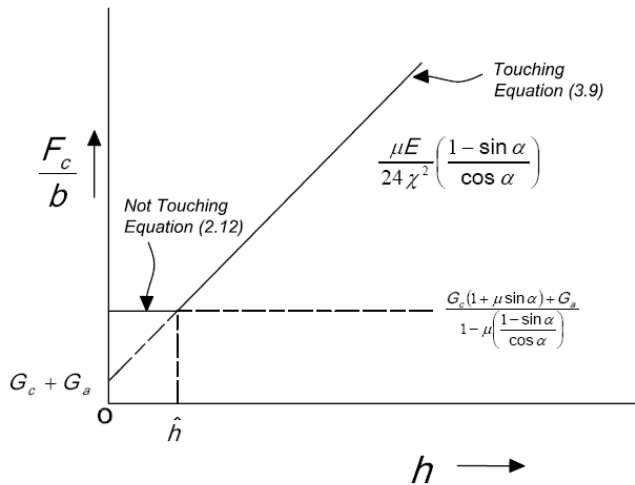


Figure 3: Force per unit width as a function of cut thickness for elastic cutting.

### Plastic Bending

In many cutting and machining operations the yield stress of the material is exceeded during the formation of the chip which results in a permanent curvature or curling. The most common manifestation of this is the curling of thin wood shavings during planing. The yielding is modelled here by assuming no work hardening, such that for:

$$e \leq e_y, \sigma = Ee$$

i.e. linear elasticity as assumed in the previous sections and for:

$$e \geq e_y, \sigma = \sigma_y$$

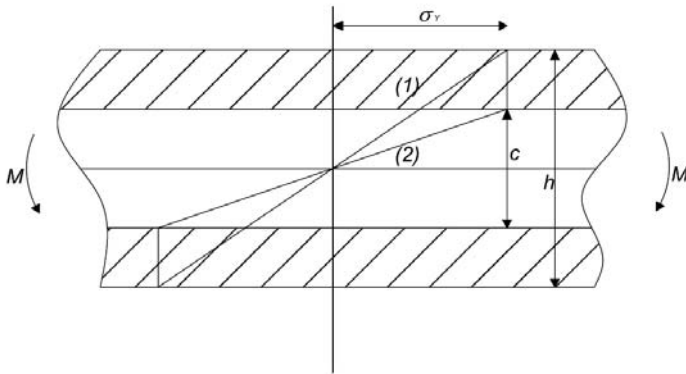


Figure 4: Stress distributions in the chip for plastic bending.

The stress distributions for plastic bending are shown in Figure 4. The distribution shown as line (1) is for first yielding and the strain at the outer surface is,

$$e_y = \frac{\sigma_y}{E} = \frac{h}{2R_p}$$

where  $R_p$  is the minimum radius for elastic deformation.

The moment to give this condition is,

$$\frac{M}{b} = \frac{\sigma_y h^2}{6}$$

and for moments greater than this value the plastic regions spread inwards giving an elastic zone of width  $c$  such that,

$$\frac{M}{b} = \frac{\sigma_y h^2}{4} \left( 1 - \frac{1}{3} \left( \frac{c}{h} \right)^2 \right) \quad (4.1)$$

At the interface the strain is  $e_y$  so that,

$$e_y = \frac{c}{2R}$$

where  $R$  is the current radius of curvature ( $R < R_p$ ) and hence,

$$\frac{M}{b} = \frac{\sigma_y h^2}{4} \left( 1 - \frac{1}{3} \left( \frac{R}{R_p} \right)^2 \right) \quad (4.2)$$

where

$$\frac{\sigma_Y h^2 b}{4} = M_p \text{ is the plastic collapse moment when } c = 0.$$

This form of analysis is widely used in analysing plastic bending in fracture tests, particularly peeling [14].

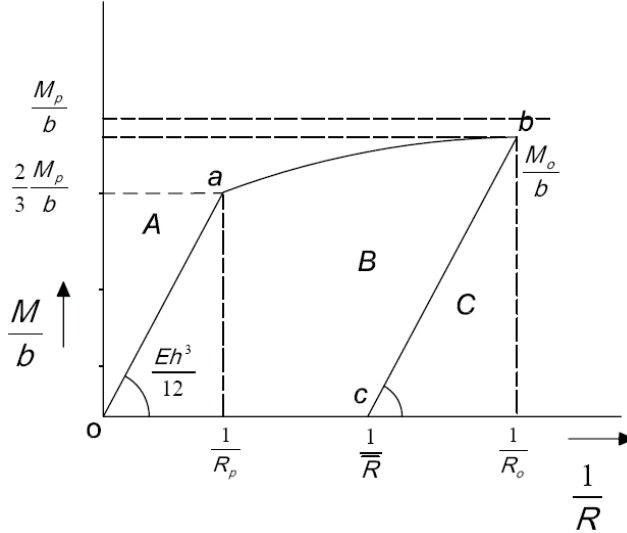


Figure 5: Relationship between radius of curvature and bending moment.

The moment-radius of curvature relationship for plastic bending is shown in Figure 5. For  $\frac{1}{R} < \frac{1}{R_p}$  we have the elastic form from equation (2.8) i.e.  $0-a$  and for  $\frac{1}{R} > \frac{1}{R_p}$ ,  $a-b$  we have the line from equation (4.2). The line  $0ab$  represents the initial bending up to the moment at point  $0$  in Figure 2 i.e.  $M_0$ . For the steady state, the unloading to point  $A$  in Figure 2 is the line  $b-c$  in Figure 5 which is parallel to  $0-a$  and at  $A$ , when  $\frac{M}{b} = 0$ , has the residual curvature of  $\frac{1}{R}$  given by

$$\frac{1}{R} = \frac{1}{R_0} - \frac{12}{Eh^3} \left( \frac{M_0}{b} \right) \tag{4.3}$$

The elastic unloading is governed by the same equations as used in the elastic case and equation (2.9) now has the boundary condition that  $R = \bar{R}$  at  $\psi = \frac{\pi}{2} - \alpha$  and hence

$$\frac{Eh^3}{24} \left( \frac{1}{R^2} - \frac{1}{\bar{R}^2} \right) = \frac{F_c}{b} (\cos \psi - \sin \alpha) + \frac{F_t}{b} (\sin \psi - \cos \alpha)$$

At  $\psi = \theta_0 \ll 1$ ,  $R = R_0$  as before and we have:

$$\frac{Eh^3}{24} \left( \frac{1}{R_0^2} - \frac{1}{\bar{R}^2} \right) - \frac{F_t}{b} \theta = \frac{F_c}{b} (1 - \sin \alpha) - \frac{F_l}{b} \cos \alpha$$

and on substituting for  $\bar{R}$  from equation (4.3) we have

$$\left( \frac{M_0}{b} \frac{1}{R_0} \right) - \frac{6}{Eh^3} \left( \frac{M_0}{b} \right)^2 - \frac{F_t}{b} \theta = \frac{F_c}{b} (1 - \sin \alpha) - \frac{F_l}{b} \cos \alpha$$

The first term is the area  $A+B+C$  in Figure 5 and the second term is the area  $C$  so the two terms give  $A+B$ . For an elastic relationship this reduces to,

$$G_b = \frac{6}{Eh^3} \left( \frac{M_0}{b} \right)^2 = \frac{Eh^3}{24} \left( \frac{1}{R_0^2} \right)$$

but for the elastic-plastic case equation (4.2) must be used,

$$\hat{G} \left( 1 - \frac{1}{3k_0^2} \right) \left[ k_0 - \frac{3}{4} \left( 1 - \frac{1}{3k_0^2} \right) \right] - \frac{F_t}{b} \theta = \frac{F_c}{b} (1 - \sin \alpha) - \frac{F_l}{b} \cos \alpha$$

where

$$\hat{G} = \frac{\sigma_y^2 h}{2E} \quad \text{and} \quad k_0 = \frac{R_p}{R_0}$$

The left hand side of this equation does not give  $G$  because the area  $B$  is the energy dissipated plastically or is stored as residual stress. The energy release rate from bending is given by area  $A$  and is,

$$G_b = \hat{G} \left( 1 - \frac{2}{3k_0} \right)$$

This may be written as

$$G + \hat{G} \gamma_1 = \frac{F_c}{b} (1 - \sin \alpha) - \frac{F_l}{b} \cos \alpha \tag{4.4}$$

and

$$G = G_b - \frac{F_l}{b} \theta = \hat{G} \gamma_2 - \frac{F_l}{b} \theta \tag{4.5}$$

where

$$\gamma_1 = \left( 1 - \frac{1}{k_0} \right)^2 \left[ k_0 + \frac{1}{4} \left( 1 - \frac{2}{k_0} \right) \left( 1 + \frac{1}{3k_0} \right) \right] \tag{4.6}$$

and

$$\gamma_2 = 1 - \frac{2}{3k_0} \quad (4.7)$$

Note that  $k_0 = 1$  is the limit of the elastic case and  $\gamma = 0$  with  $\gamma_2 = \frac{1}{3}$ , i.e.  $G_b = \frac{\hat{G}}{3}$ . For  $k_0 \rightarrow \infty$ ,  $\gamma_1 \rightarrow \infty$  and  $\gamma_2 = 0$ , i.e.  $G_b \rightarrow \hat{G}$ .

It should be noted that the first part of  $\gamma_1$ , i.e.  $k_0 \left(1 - \frac{1}{k_0}\right)^2$  is the plastic energy dissipation and the second, i.e.  $\frac{1}{4} \left(1 - \frac{1}{k_0}\right)^3 \left(1 + \frac{1}{3k_0}\right)$  is that stored elasticity in the curled chip. For  $k_0 \gg 1$  the former is much the larger part.  $\frac{F_t}{b}$  may now be determined from equation 2.5,

$$\frac{F_t}{b} = Z \frac{F_c}{b} + \frac{G_a}{\cos \alpha + \mu \sin \alpha}$$

$$\text{and also } \theta_0 = \frac{\chi h}{R_0} = 2\chi e_\gamma k_0$$

The form of the solution may be seen more easily when the friction conditions are ignored, i.e.  $\mu = G_a = 0$  and hence  $Z = -\tan \alpha$  and if we assume that  $G = G_c$  then,

$$\begin{aligned} \frac{F_c}{bG_c} &= 1 + \frac{\hat{G}}{G_c} \gamma_1 \\ \frac{\hat{G}}{G_c} &= \frac{1 - \gamma_3 k_0}{\gamma_2 + \gamma_1 \gamma_3 k_0} \end{aligned} \quad (4.8)$$

where  $\gamma_3 = 2\chi e_\gamma \tan \alpha$ .

Since  $k_0 \geq 1$  for plasticity to occur then  $\gamma_2 < 1$ . For  $\gamma_3 \geq 1$  then  $\hat{G} = 0$  and  $\frac{F_c}{b} = G_c$ , the elastic case. This limit is reached when:

$$\tan \alpha = \frac{1}{2\chi e_\gamma}$$

$2\chi e_\gamma$  is generally small and  $\alpha$  would be very close to  $\frac{\pi}{2}$  for this condition to occur. For most cases  $\gamma_3$  is small and the limiting case is zero when there is no root rotation.  $G$  is then limited to  $\hat{G}$  when  $\gamma_2 = 1$  and  $\gamma_1 \rightarrow \infty$ .

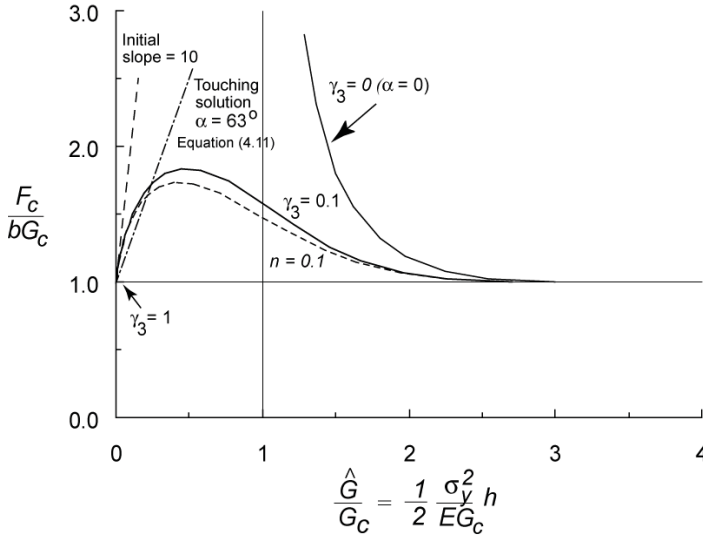


Figure 6: Plastic bending case for  $\mu = G_a = 0$  for  $\gamma_3 = 2\chi e_\gamma \tan \alpha$

Figure 6 shows  $\frac{F_c}{bG_c}$  versus  $\frac{\hat{G}}{G_c}$  for  $\gamma_3 = 0$  and there are no solutions for  $\frac{F_c}{bG_c}$  when  $\frac{\hat{G}}{G_c} < 1$ ; i.e. it is not possible to achieve cutting in this mode. The line for  $\gamma_3 = 0.1$  ( $\alpha \approx 70^\circ$ ) is also shown and now there are values in the range  $0 < \frac{\hat{G}}{G_c} < 2.7$ . For  $\frac{\hat{G}}{G_c} > 2.7$  elastic cutting occurs. There is a maximum in the force at  $\frac{\hat{G}}{G_c} \approx 1.2$ , i.e.  $h = \hat{h} = \frac{EG_c}{\sigma_y^2}$  with a value of  $\frac{F_c}{bG_c} = \frac{1}{2} \left( 1 + \sqrt{\frac{1}{\gamma_3} + 1} \right) \approx 2.2$ . At small values of  $\frac{\hat{G}}{G_c}$ , i.e. low values of  $h$ , the curve becomes linear with a slope of  $\gamma_3^{-1}$  and we have

$$\frac{F_c}{h} = G_c + \frac{\sigma_y}{4\chi \tan \alpha} h \quad (4.9)$$

This form of curve is quite commonly observed in fracture involving plasticity in which the plastic energy maximises at some fraction of the plastic zone size; i.e.  $r_p = \frac{1}{2\pi} \frac{EG_c}{\sigma_y^2}$ , and gives elastic behaviour at each end; i.e.  $h=0$  and  $h \approx \frac{6EG_c}{\sigma_y^2}$ .

The crack tip touching condition is more closely modelled by equation (3.5) in this case, since  $\frac{1}{R}$  decreases to  $\frac{1}{R}$  and not zero as in the elastic case. A similar analysis to the elastic one using  $\bar{\theta}_0 = \frac{1 - \sin \alpha}{\cos \alpha}$  for which

$$\bar{k}_0 = \frac{1}{\gamma_3} \frac{\sin \alpha}{1 + \sin \alpha} \quad (4.10)$$

which remains constant for all loads in the touching condition. For the case of  $G=G_c$  we have,

$$\frac{F_c}{b} = G_c + G_a + \hat{G} \left( \gamma_1 + \frac{\mu \cos \alpha}{1 - \sin \alpha} (\gamma_1 + \gamma_2) \right) \quad (4.11)$$

where  $\gamma_1$  and  $\gamma_2$  are evaluated at  $\bar{k}_0$ . This is the equivalent relationship to equation (3.9) and is linear in  $h$ . An example of the solution is shown in Figure 6 in which  $2\chi e_y = 0.05$  is used so that, with  $\gamma_3 = 0.1$ ,  $\tan \alpha = 2$ , i.e.  $\alpha = 63^\circ$  for which  $\bar{k}_0 = 4.7$ . The straight line is for equation (4.11) for  $\mu = G_a = 0$  and the intersection of the lines is at the onset of touching. Thus the initial linear behaviour is at a reduced slope and then moves to the non-touching curve for higher thicknesses. For high  $\bar{k}_0$  values the linear relationship approximates to,

$$\frac{F_c}{b} = (G_c + G_a) + \frac{\sigma_y}{4\chi} \left( \frac{1 - \sin \alpha}{\cos \alpha} + \mu \right) h \quad (4.12)$$

which may be compared to equation (4.9).

The limitations of this solution are apparent for low  $\alpha$  values for which  $\alpha = 0$  gives  $\gamma_3 = 0$  and the line is shown in Figure 6 with no solution for  $\hat{G} < G_c$ . The touching solution gives

$$\bar{k}_0 = \frac{1}{2\chi e_y}$$

and hence a  $\bar{k}_0$  value of 20 for the example used here. This gives strains much larger than 0.15 and a very steep line in Figure 6. For all cases when  $\alpha$  is less than  $70^\circ$  bending requires such high strains and therefore the process would not occur. However an alternative plastic deformation mode is available which will now be considered.

### Plastic Shearing

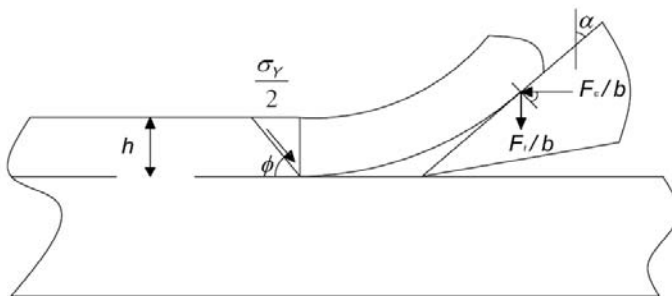


Figure 7: Plastic shearing.

The additional plastic deformation mode is shown in Figure 7 in which the shear stress on a plane inclined at an angle  $\phi$  reaches the shearing yield stress  $\frac{\sigma_Y}{2}$  using the Tresca yield criterion. Equilibrium of forces gives,

$$\frac{\sigma_Y}{2} \frac{h}{\sin \phi} = \frac{F_c}{b} \cos \phi - \frac{F_t}{b} \sin \phi \quad (5.1)$$

This form of deformation has been widely studied in the metals machining literature and in particular by Merchant [15] who proposed that  $\phi$  was determined by minimising the force  $F_c$ . The shear deformation can be seen in the cutting of many materials. By use of equation (2.5) we can eliminate  $F_t/b$ :

$$\frac{F_c}{b} = \frac{1}{(1-Z \tan \phi)} \left( \frac{\sigma_Y h}{2} \frac{1}{\tan \phi} + \left( \frac{\sigma_Y h}{2} + \frac{G_a}{\cos \alpha + \mu \sin \alpha} \right) \tan \phi \right) \quad (5.2)$$

Differentiating with respect to  $\tan \phi$  gives a minimum condition for  $\phi$  defined by

$$(1+H) \tan^2 \phi_0 + 2Z \tan \phi_0 - 1 = 0 \quad (5.3)$$

i.e.

$$\tan \phi_0 = \frac{\sqrt{1+Z^2+H} - Z}{1+H}$$

and

$$\cot \phi_0 = \sqrt{1+Z^2+H} + Z$$

where

$$H = \frac{2G_a}{\sigma_Y h (\cos \alpha + \mu \sin \alpha)}$$

On substituting in equation (5.2) we have the minimum in  $\frac{F_c}{b}$ , i.e.

$$\frac{F_c}{b} = \sigma_Y h \cot \phi_0 \quad (5.4)$$

It should be noted that for  $\mu = G_a = 0$ ,

$$\cot \phi_0 = -\tan \alpha + \sqrt{1 + \tan^2 \alpha} = \frac{1 - \sin \alpha}{\cos \alpha} \text{ i.e. } \phi_0 = \frac{\pi}{4} + \frac{\alpha}{2} \quad (5.5)$$

an expression familiar from previous sections.

The extreme form of shear deformation is shown in Figure 8 in which the chip rotates through an angle  $\left(\frac{\pi}{2} - \alpha\right)$  and the tool fits into the gap as shown.

Continuity requires that for plane strain the chip thickness changes and we have

$$h_c = h \frac{\cos(\phi_0 - \alpha)}{\sin \phi_0} \quad (5.6)$$

and a shear strain is induced of,

$$e_s = \frac{\cos \alpha}{\sin \phi_0 \cos(\phi_0 - \alpha)} \quad (5.7)$$

It should be noted that for no thickness change,  $h_c = h$ ,  $\cot \phi_0 = \frac{1 - \sin \alpha}{\cos \alpha}$ , i.e. the zero friction condition.

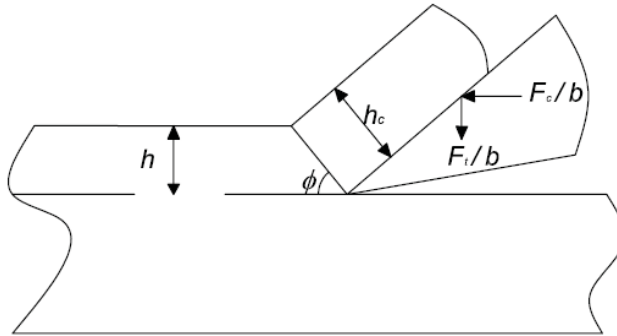


Figure 8: Plastic shearing with no bending.

This is a crack tip touching case and hence the fracture solution may be obtained by simply adding  $G_c$  to equation (5.4), i.e.,

$$\frac{F_c}{b} = G_c + \sigma_Y h \cot \phi_0 \quad (5.8)$$

For the zero friction case equation (5.5) can be used to give:

$$\frac{F_c}{b} = G_c + \left( \frac{1 - \sin \alpha}{\cos \alpha} \right) \sigma_Y h \quad (5.9)$$

On comparing with equation (4.12) for the bending situation with crack tip touching, it can be seen that the latter gives an identical form but with a lower slope. Thus the bending mode, if possible, would be preferred but for low  $\alpha$  it is not and shearing occurs. For the general case,

$$\frac{F_c}{b} = G_c + \sigma_Y h \left( Z + \sqrt{1 + Z^2 + \frac{2G_a}{\sigma_Y h (\cos \alpha + \mu \sin \alpha)}} \right) \quad (5.10)$$

which is non-linear in  $h$  and extrapolates to  $G_c$  at  $h = 0$  and has the form,

$$\frac{F_c}{b} = G_c + \sqrt{\frac{2\sigma_y h G_a}{\cos \alpha + \mu \sin \alpha}} \text{ for small } h.$$

For large  $h$  there is a linear form,

$$\frac{F_c}{b} \approx G_c + \frac{G_a}{\sqrt{1+\mu^2}} + \left( \frac{1-\sin(\alpha-\beta)}{\cos(\alpha-\beta)} \right) \sigma_y h \quad (5.11)$$

where  $\tan \beta = \mu$ .

If touching is not assumed then the expression for  $\frac{F_c}{b}$ , equation (5.2), becomes

$$\frac{F_c}{b} = \frac{1}{(1-Z \tan \phi)} \left( \frac{\sigma_y h}{2} \frac{1}{\tan \phi} + \left( \frac{\sigma_y h}{2} + \frac{G_a}{\cos \alpha + \mu \sin \alpha} + G_c \tan \alpha \right) \tan \phi + G_c \right) \quad (5.12)$$

The condition for minimum  $\frac{F_c}{b}$  is now,

$$\left( 1 + H + \frac{2(Z + \tan \alpha)G_c}{\sigma_y h} \right) \tan^2 \phi_0 + 2Z \tan \phi_0 - 1 = 0$$

and is given by,

$$\frac{F_c}{b} = \sigma_y h \cot \phi_0 + G_c$$

as before with,

$$\cot \phi_0 = \sqrt{1 + Z^2 + \frac{2}{\sigma_y h} \left( \frac{G_a + \frac{\mu G_c}{\cos \alpha}}{\cos \alpha + \mu \sin \alpha} \right)} + Z \quad (5.13)$$

This is the same solution, though in a different form, as that given by Atkins [10] with  $G_a=0$ .

The solution gives  $\frac{F_c}{b} = G_c$  for  $h=0$  and has a  $\sqrt{h}$  form at low  $h$  as in equation (5.10). For large  $h$  we again have a linear relationship

$$\frac{F_c}{b} = G_c \left( 1 + \frac{\mu}{\sqrt{1+\mu^2}} \frac{1}{\cos \alpha} \right) + \frac{G_a}{\sqrt{1+\mu^2}} + \left[ \frac{1-\sin(\alpha-\beta)}{\cos(\alpha-\beta)} \right] \sigma_y h \quad (5.14)$$

i.e. an identical slope but a slightly higher intercept than equation (5.11). The general form of these results is shown in Figure 9.

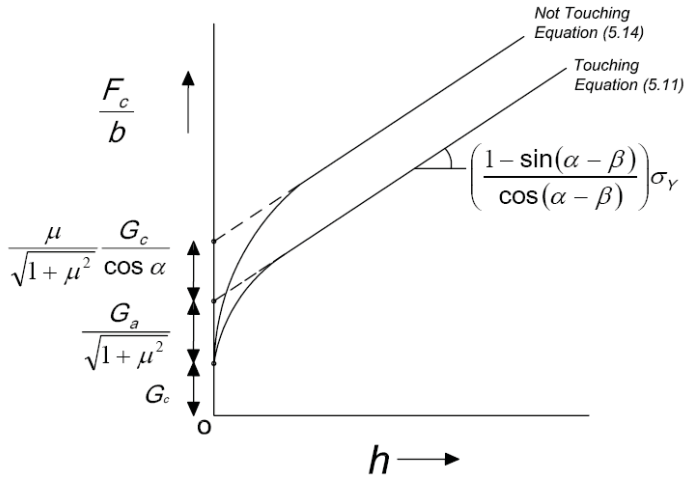


Figure 9: Fracture force per unit width as a function of thickness for shear yielding.

This analysis does not include bending but generally some will occur prior to the formation of the slip band. Thus the chip will undergo a rotation of  $\theta_0$  at the crack tip given by,

$$\sin \theta_0 = 2\chi \hat{\epsilon}$$

where  $\hat{\epsilon}$  is the maximum bending strain. The shear band angle will be reduced by  $\theta_0$  but the optimisation of  $(\phi - \theta_0)$  is the same as for  $\phi$  and equation (5.8) now becomes,

$$\frac{F_c}{b} = G_c + \sigma_Y h \left( \cot(\phi_0 - \theta_0) + \frac{\sin \theta_0}{4\chi} \right)$$

and the total plastic work increases.

The value of  $\phi_0$  at  $h \rightarrow \infty$ ,  $\bar{\phi}_0$  may be derived from equation (5.3) and is,

$$\tan \bar{\phi}_0 = \sqrt{1 + Z^2} - Z$$

and since  $Z = \tan(\beta - \alpha)$  then:

$$\tan \bar{\phi}_0 = \frac{1 - \sin(\beta - \alpha)}{\cos(\beta - \alpha)} = \tan \left[ \frac{\pi}{4} - \frac{(\beta - \alpha)}{2} \right]$$

i.e.

$$\bar{\phi}_0 = \left( \frac{\pi}{4} - \frac{\beta}{2} \right) + \frac{\alpha}{2}$$

and on including  $\theta_0$  we have:

$$\bar{\phi}_0 = \left( \frac{\pi}{4} - \frac{\beta}{2} - \theta_0 \right) + \frac{\alpha}{2}$$

If we limit  $\hat{e}$  to 0.15, i.e.  $\theta_0 = 11^\circ$  and for  $\phi_0$  values of about  $45^\circ$ , i.e. low friction cases, the energy dissipated increases by a factor of about 1.6. This, perhaps surprising, result arises from the necessity of satisfying the kinematics in forming the shear plane, i.e. some bending must precede its formation.

### Work hardening

The plasticity solution given so far has assumed a perfectly plastic material, but in some cases the occurrence of work hardening can have significant effects. Now we shall assume that:

$$e \leq e_Y, \sigma = Ee$$

and

$$e \geq e_Y, \sigma = \sigma_Y \left( \frac{e}{e_Y} \right)^n$$

in simple tension. The bending case may be analysed for this condition and equations (4.4) and (4.5) are the same but the expression for  $\gamma_1$  and  $\gamma_2$  in equations (4.6) and (4.7) become,

$$\gamma_1 = \frac{2k_0^{1+n}}{(2+n)(1+n)} + \frac{2}{3} \left( \frac{1-n}{2+n} \right) \frac{1}{k_0} - \left( \frac{1-n}{1+n} \right) - \frac{3}{4} \left[ \frac{2}{2+n} k_0^n - \frac{2}{3} \left( \frac{1-n}{2+n} \right) \frac{1}{k_0^2} \right]^2 \quad (6.1)$$

$$\gamma_2 = \left( \frac{1-n}{1+n} \right) - \frac{3}{4} \left( \frac{1-n}{2+n} \right) \frac{1}{k_0} + \frac{2n}{(2+n)(1+n)} k_0^{n+1} \quad (6.2)$$

The non-work hardening forms are retrieved for  $n=0$  and at  $k_0=1, \gamma_1=0$  and  $\gamma_2=\frac{1}{3}$ , for all  $n$ .

The effect of working hardening is illustrated in Figure 6 where the solutions for zero friction are given for equation (4.8). For  $n=0.1$  and  $\gamma_3=0.1$  it can be seen that the effect is small and does not alter the form of the solution. This is perhaps to be expected since the strains are not large in bending.

This is not so in shear yielding and here it can describe the work hardening in shear by using,

$$\sigma_s = \frac{\sigma_Y}{2} \left( \frac{3e_s}{2e_Y} \right)^n \quad (6.3)$$

where

$$e_s = \frac{\cos \alpha}{\cos(\phi_0 - \alpha) \sin \phi_0} = \frac{\tan \phi_0 + \cot \phi_0}{1 + \tan \alpha \tan \phi_0}$$

Note that for  $\phi_0 \approx \frac{\pi}{4}$  and  $\alpha = 0$ ,  $e_s = 2$  so that  $\left(\frac{3e_s}{2e_y}\right)$  would be a large number.

The equation for  $\frac{F_c}{b}$ , equation (5.2), now becomes,

$$\frac{F_c}{b} = \frac{1}{1 - Z \tan \phi} \left[ \frac{\sigma_y h}{2} \left( \frac{3e_s}{2e_y} \right)^n \left( \frac{1}{\tan \phi} + \tan \phi \right) + \frac{G_a \tan \phi}{\cos \alpha + \mu \sin \alpha} \right] \quad (6.4)$$

This may be minimised as before and for small  $n$  the solution for  $\phi_0$  is changed very little and all the results so far given apply with  $\sigma_y$  increased by the factor  $\left(\frac{3e_s}{2e_y}\right)^n$ , i.e. an enhanced yield stress.

### Experimental comparisons

A separate paper [16] will be published describing experimental work specifically designed to explore the analysis given here. There is, however, an extensive body of results in the literature and in particular [17] on machining polymers and [8] on metals. Both tabulate the values of  $F_c$ ,  $F_t$  and  $\phi_0$  for a range of  $h$  and  $\alpha$  values so that it is possible to perform direct comparisons with the analysis.

A set of data from Kobayashi [17] is given, for six polymers, in Table 2. The first analysis performed concerned the assumptions about friction on the tool face which are embodied in equation (2.5). For the crack tip touching condition the extra term,  $-ZG_c$ , is included and the analysis as shown in equation (7.1):

$$\frac{F_t}{b} = Z \frac{F_c}{b} + \frac{G_a}{\cos \alpha + \mu \sin \alpha} - ZG_c \quad (7.1)$$

This assumes a linear dependence of  $\frac{F_t}{b}$  on  $\frac{F_c}{b}$  with a positive intercept. The six sets of data are shown in Figure 10 and good linearity is apparent and the values of  $Z$ ,  $\mu$  and the intercept:  $G_1 = \frac{G_a}{\cos \alpha + \mu \sin \alpha} - ZG_c$ , are also given in Table 2.  $G_1$  is always positive and illustrates the importance of including  $G_a$  in the friction model. Figure 11 shows  $\frac{F_c}{b}$  versus  $h$  and the lines are fitted using equation (5.10) for the crack tip touching case. The solver function in Microsoft Excel™ was used to accommodate the non-linearity and the fit gives two parameters since  $G_1$ ,  $Z$  and  $\mu$  are known from Figure 10 and hence  $G_c$ ,  $G_a$  and  $\sigma_y$  are found. These values are also shown in Table 2. The non-touching case, which has  $\cot \phi_0$  given in equation (5.13), has the same form as equation (5.10) so that the non-linear fit will give the same value of  $G_c$  but  $G_a$  is found directly from equation (7.1) since the  $ZG_c$  term is omitted. The  $G_a$  value is given as  $\bar{G}_a$  in Table 2 and is slightly changed.

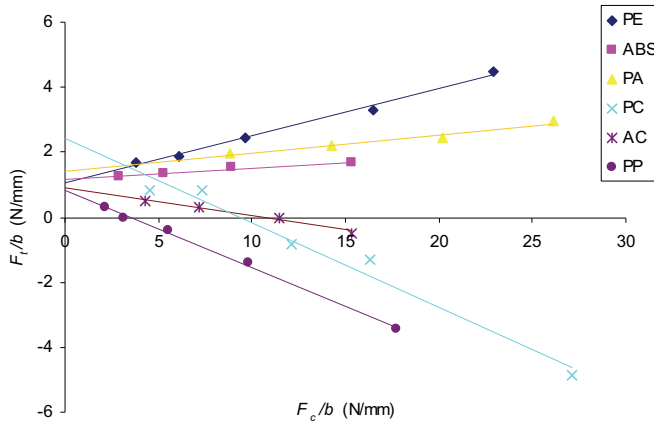


Figure 10: Polymer data from [17]; Transverse force per unit width as a function of cutting force for various polymers. Equation (2.5) is fitted.

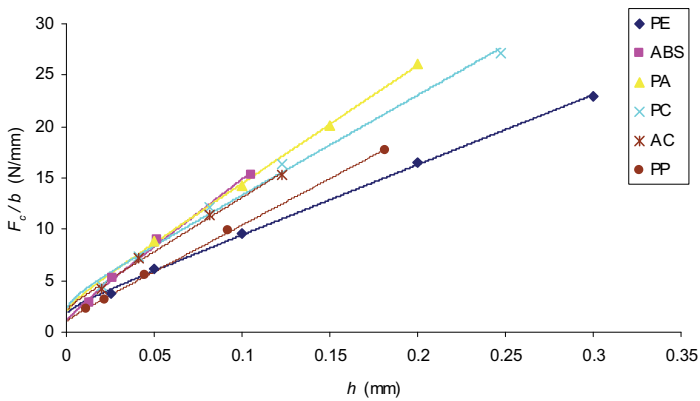


Figure 11: Polymer data from [17]; Cutting force per unit width as a function of thickness of cut for various polymers. Equation (5.10) is fitted.

Table 2: Results from the analysis of the machining data for polymers from [17]. (Note that the values of  $\sigma_Y$  in brackets are taken from [17]).

Material	$h$ (mm)	$\bar{\tau}$ ( $\text{Nmm}^{-1}$ )	$\bar{\tau}$ ( $\text{Nmm}^{-1}$ )	$\bar{\phi}$	$\phi^\circ$	$Z$	$G_I$ ( $\text{kJm}^{-2}$ )	$\mu$	$G_c$ ( $\text{kJm}^{-2}$ )	$\sigma_Y$ (MPa)	$G_a$ ( $\text{kJm}^{-2}$ )	$\bar{\sigma}$ ( $\text{kJm}^{-2}$ )
PE $\alpha = 0^\circ$	0.025	3.78	1.70		20.5							
	0.05	6.17	1.89		28.0							
	0.10	9.64	2.46	40.6	33.0	0.15	1.05	0.15	1.46	59 (20)	1.27	1.05
	0.20	16.63	3.31		35.1							
ABS $\alpha = 10^\circ$	0.30	23.06	4.54		33.8							
	0.013	2.87	1.27		39.2							
	0.026	5.32	1.35	44.0	39.2	0.035	1.17	0.21	0.62	126 (30)	1.22	1.15
	0.052	8.96	1.52		41.3							
PA $\alpha = 10^\circ$	0.105	15.38	1.69		43.4							
	0.05	8.82	1.96		46.8							
	0.10	14.21	2.21	43.4	46.1	0.056	1.43	0.23	1.58	108 (55)	1.55	1.40
	0.15	20.09	2.45		46.1							
PC $\alpha = 20^\circ$	0.20	25.97	2.94		46.0							
	0.020	4.56	0.82		40.3							
	0.041	7.34	0.82		44.7							
	0.082	12.23	-0.82	52.3	46.6	-0.26	2.42	0.096	1.68	125 (50)	1.93	2.49
AC $\alpha = 10^\circ$	0.123	16.30	-1.31		47.5							
	0.247	27.22	-4.89		48.5							
	0.020	4.25	0.49		36.6							
	0.041	7.19	0.33	47.5	39.0	-0.088	0.92	0.088	1.82	115 (70)	0.76	0.92
PP $\alpha = 20^\circ$	0.082	11.45	0	41.2	41.2							
	0.123	15.37	-0.49		41.8							
	0.11	2.18	0.30		40.2							
	0.022	3.17	0		46.7							
Note: PE – Polyethylene PA – Polyamide AC – Polyacetal	0.045	5.54	-0.40	51.7	49.9	-0.24	0.85	0.12	0.69	114 (30)	0.67	0.87
	0.092	9.80	-1.39		52.4							
	0.182	17.33	-3.37		49.0							

Note: PE – Polyethylene  
 PA – Polyamide  
 AC – Polyacetal  
 ABS – Acrylo-Butadiene-Styrene  
 PC – Polycarbonate  
 PP – Polypropylene

The values derived for  $G_c$  cannot be checked but are reasonable for the polymers. i.e. ABS and PP give rather low values while PE, PC, PA and AC are all similar [18]. There is nothing to compare with  $G_a$  other than  $G_c$  and they have similar values which may be because the chips are adhered to the tool and are then sheared to failure. The  $\sigma_Y$  values are all rather high although, again, there is no way of knowing the true values. Some values are given in [17] and are shown in brackets in Table 2. The ratios range from 1.6 (AC) to 4.2 (ABS) and perhaps suggest that work hardening is present. This ratio is  $\left(\frac{3 e_s}{2 e_Y}\right)^n$  as given in equation (6.6).

Some further insight is provided by the  $\phi_0$  values which are derived from measuring  $h_c$  and using equation (5.6), ie

$$\tan \phi_0 = \frac{\cos \alpha}{\frac{h_c}{h} - \sin \alpha}$$

In all cases, other than PA,  $\phi_0$  in Table 2 can be seen to increase with  $h$  as is expected from equation (5.3), for which the solution for small  $h$  is,

$$\tan \phi_0 = \tan \bar{\phi}_0 - \frac{G_a \tan^2 \bar{\phi}_0}{b_Y \sqrt{1 + \mu^2}} h^{-1} = \tan \bar{\phi}_0 - \frac{\bar{h}}{h} \tag{7.2}$$

where

$$\tan \bar{\phi}_0 = \sqrt{1 + Z^2} - Z$$

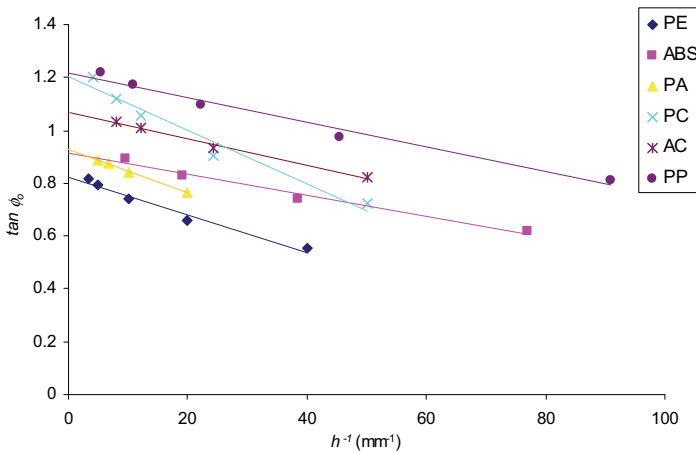


Figure 12: Shear plane angle as a function of inverse cut thickness for various polymers. Data is from [17]. Equation (7.2) is fitted.

Figure 12 shows  $\tan \phi_0$  as a function of  $h^{-1}$  and most of the data give a reasonably linear fit. The experimental values of  $\bar{\phi}_0$  and  $\bar{h}$  are compared to those derived from equations (7.2) in Table 3.

The  $\bar{\phi}$  values agree quite well and are generally lower in the experiments. This is consistent with the notion of  $\theta_0$  affecting  $\bar{\phi}_0$  and Table 3 gives values of  $\theta_0$  of about  $4^\circ$  in some cases. The  $\bar{h}$  values are generally much lower than those predicted.

Table 3: Machining Data for Polymers from [17].

$V$ (ms <sup>-1</sup> )	Material	Predicted		Experimental		$\theta_0$
		$\bar{\phi}$	$\bar{h}$ ( $\mu$ m)	$\bar{\phi}$	$\bar{h}$ ( $\mu$ m)	
0.4	PE	40.6	16	36.9	10	4
2.5	ABS	44.0	9	44.1	4	~0
1.7	PA	43.4	12	46.1	-1	-3
3.3	PC	52.3	26	48.5	6	4
6.7	AC	47.5	8	42.3	4	5
6.7	PP	51.7	10	52.2	5	~0

There are some uncertainties about determining  $\bar{\phi}_0$  from  $h_c$  in polymers since the machining speeds are high (typically 2-7 ms<sup>-1</sup>) and lead to considerable heating in the chips. Simple thermal calculations would suggest temperature rises of up to 70°C in most cases which could cause  $h_c$  to recover considerably. This probably explains the rather large variation in the measurements. However, if  $\theta_0 \cong 5^\circ$  is assumed then the  $\sigma_\gamma$  and  $\bar{h}$  values are reduced by about 20%.

It should also be noted that the chip thickness changes used to determine  $\phi_0$  experimentally confirm that shear yielding is occurring since bending deformation alone would give no change from cut thickness to chip thickness. The bending solution equations (3.9) and (4.11) both give a linear dependence of  $\frac{F_c}{b}$  vs  $h$ , but the measured slopes give unrealistic values of  $E$  and  $\sigma_\gamma$ .

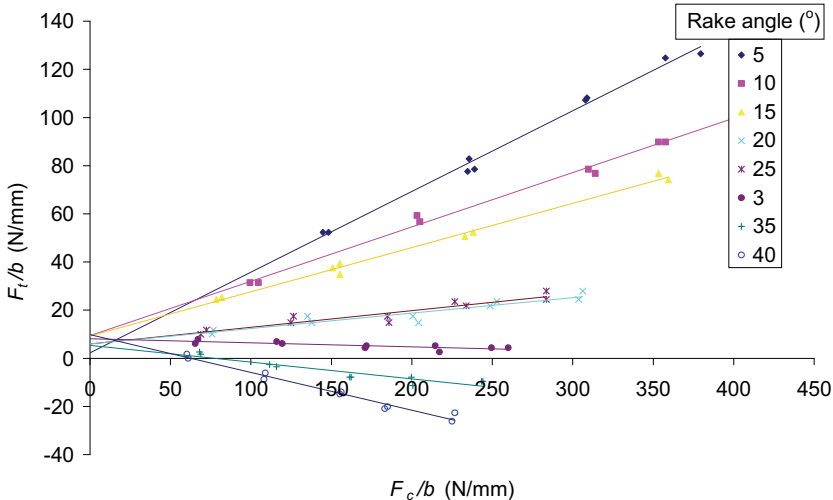


Figure 13: Transverse force as a function cutting force per unit width for steel [8].

Equation (2.5) is fitted.

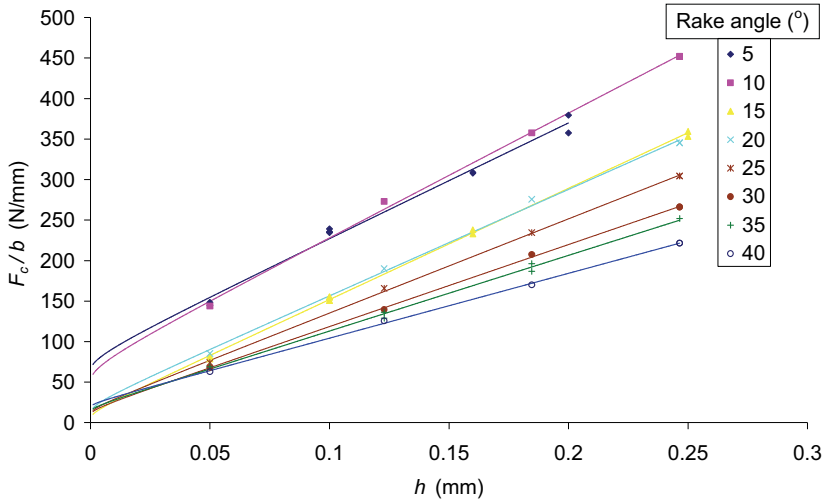


Figure 14: Cutting force per unit width as a function of thickness of cut for steel at various rake angles [8]. Equation (5.10) is fitted.

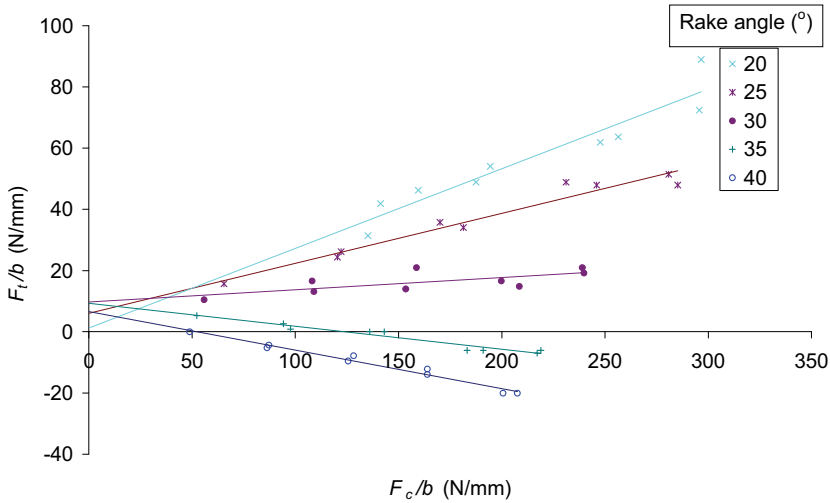


Figure 15: Transverse force as a function cutting force per unit width for  $\alpha$ -brass at various rake angles [8]. Equation (2.5) is fitted.

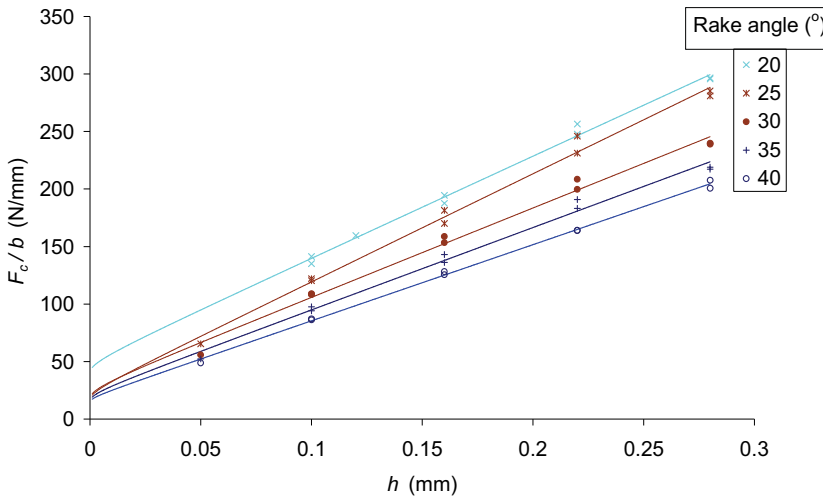


Figure 16: Cutting force per unit width as a function of thickness of cut for  $\alpha$ -brass at various rake angles [8]. Equation (5.10) is fitted.

Some data taken from [8] for a steel [SAE1112] and an  $\alpha$ -brass containing 15% Zn are shown in Figures 13-16. The  $\frac{F_c}{b}$  vs  $\frac{F_c}{b}$  results are for different  $\alpha$  values and show good linearity with clear positive intercepts. The values of  $\mu$ ,  $\sigma_Y$ ,  $G_a$ ,  $G_c$  and  $\bar{h}$  are given in Table 4. It would be expected that  $G_c$  would be independent of  $\alpha$  and, while this is true for higher  $\alpha$  values, the value is significantly above the average at the lowest  $\alpha$  value. Indeed all the parameters are sensibly independent of  $\alpha$  for most of the range as expected from the analysis. The  $G_c$  and  $G_a$  values, which have standard deviations of about  $\pm 1 \text{ kJm}^{-2}$ , are very similar for the two metals. The  $\mu$  values are much higher than for polymers and the yield stresses are factors of 2-3 higher than first yield values, as with polymers.

The  $\phi_0$  values were meticulously measured in [8] using three different dimensional changes, i.e. the thickness as in [17], but also using the chip width and the axial length.  $\phi_0$  does changes with  $h$  but only slowly and the measured  $\bar{h}$  values are given in Table 5 together with the predicted values.

As for polymers, the measured  $\bar{h}$  values are significantly less than predicted, i.e. an average measured value of 2-3  $\mu\text{m}$  compared to predicted values of 8-11  $\mu\text{m}$ . The measured  $\bar{\phi}_0$  values are given in Table 5 together with the predictions and here the experimental values are again lower than the predicted values. The  $\theta_0$  values are also given and are reasonably constant at  $19^\circ$  for steel and  $16.5^\circ$  for brass, i.e. implying strains of about 24%. If the  $\phi_0$  values for both metals are decreased by  $18^\circ$ , the  $\sigma_Y$  and  $\bar{h}$  values decrease by about a factor of two. Thus the yield stresses are about 500MPa for steel and 320 MPa for brass which are much closer to the accepted values, though, they do probably still reflect considerable work hardening. The  $\bar{h}$  values predicted are also closer to the experimentally measured values.

Table 4: Results obtained for the metals cutting data, from [8].

Steel						
$\alpha (^{\circ})$	$\mu$	$\sigma_Y$ (MPa)	$G_a$ (kJm <sup>-2</sup> )	$G_c$ (kJm <sup>-2</sup> )	$\bar{h}$ ( $\mu\text{m}$ )	(experimental) $\bar{h}$ ( $\mu\text{m}$ )
5	0.44	1020	24.8	64.4	11	5
10	0.41	1250	17.5	26.2	8	1
15	0.47	1140	11.2	5.0	6	3
20	0.52	1000	7.8	14.0	5	3
25	0.56	970	6.5	14.0	5	2
30	0.56	960	8.8	14.0	8	1
35	0.60	940	4.6	21.2	5	3
40	0.49	950	8.2	16.5	13	3
Average	0.51	1030	11.2	22.0	8	3

$\alpha$ - brass						
$\alpha (^{\circ})$	$\mu$	$\sigma_Y$ (MPa)	$G_a$ (kJm <sup>-2</sup> )	$G_c$ (kJm <sup>-2</sup> )	$\bar{h}$ ( $\mu\text{m}$ )	(experimental) $\bar{h}$ ( $\mu\text{m}$ )
20	0.69	680	13.6	41.0	10	3
25	0.68	800	11.0	16.9	18	1
30	0.62	750	13.2	18.1	14	3
35	0.59	770	9.8	15.5	12	2
40	0.65	750	5.2	15.4	9	2
Average	0.65	750	10.6	21.4	11	2

Table 5: Shear plane angles for  $\alpha$ -brass and steel [8].

$\alpha$	$\alpha$ - brass			Steel		
	$\bar{\phi}_o$	$\bar{\phi}_o$ (experimental)	$\theta_o$	$\bar{\phi}_o$	$\bar{\phi}_o$ (experimental)	$\theta_o$
5	-	-	-	35.7	15.7	20.0
10	-	-	-	38.9	16.5	22.4
15	-	-	-	39.9	20.6	19.3
20	37.5	21.7	15.8	41.3	25.4	15.9
25	40.5	22.7	17.8	42.9	28.5	14.4
30	44.0	24.8	19.2	45.4	32.3	13.1
35	47.0	26.8	20.2	47.0	34.5	12.5
40	50.0	28.0	22.0	52.0	37.8	14.2
Average			19			16.5

### Conclusions

The analysis presented here makes three additions to the established machining and cutting literature as well as incorporating fracture toughness as advocated by Atkins [10]. The analysis has

been applied to published machining data, i.e. to polymer machining data published by Kobayashi [17] and metals machining data published by Eggleston et al [8].

The first analytical development was to incorporate into the friction model a term  $G_a$  which may be interpreted as an initiation or adhesion shear condition at the interface. The experimental data analysed for both polymers and metals clearly shows that this term is essential and results in values of the coefficient of friction between the tool and the chip,  $\mu$ , being independent of thickness. The  $G_a$  values are of a similar magnitude to  $G_c$  in the data examined and both  $G_a$  and  $G_c$  are mostly independent of rake angle. However, at low values of rake angle there is some evidence of higher values of  $G_c$  and  $G_a$  which may be a consequence of mixed mode effects [19]. The reliability of the  $G_c$  values makes a cutting or machining procedure a possible route for measuring toughness in highly ductile materials and this notion will be explored elsewhere [16].

The second development was the incorporation of root rotation during bending into the analysis. For elastic and elastic-plastic chip bending this leads to solutions for  $G_c$  which describe cutting under such conditions. However, this analysis shows that the bending mechanisms are, in general, inefficient and apply only under limited circumstances, i.e. at high rake angles.

The third development arises here since to generate sufficient energy release rate one must postulate that the tool tip touches the crack tip and energy is put directly into the fracture. Such a model removes the requirement for a crack to exist ahead of the tool, a limitation that bedevilled early attempts to use a fracture based analysis to describe cutting. These bending solutions are only feasible for large rake angles ( $>60^\circ$ ) and for smaller values the well established shear plane deformation must be invoked. This is done here using Merchant's force minimisation method but incorporating root rotation.

The experimental data for both polymers and metals fit the general form of the analysis quite well but the yield stress values are generally much higher than first yield and suggest considerable work hardening during the shearing. They are generally independent of rake angle. The shear plane angles have been closely studied in the past and much has been made of the fact that the predictions are generally higher than the measurements. In the data used here this was again found to be true although the increase of angle with thickness is predicted via  $G_a$ . The discrepancy in angle does correlate reasonably well with the idea that it corresponds to root rotation though this conclusion requires further evidence. This is particularly so in polymer data where recovery effects may cause problems with the angle measurements. There is significant evidence that work hardening results in high yield stress values, particularly in the case of polymers. The presence of this rotation also provides a description of bending effects in the shear case. The simple Merchant model does not include such effects which are observed as chip curling. The observation also suggests that the bending strains are limited to about 6% in polymers but up to 20% in metals. It is unclear if this is a consequence of limitations in the bending process such as compression buckling or from cracking in the chip.

## References

- (1) Mallock A. The action of cutting tools. *Proceedings of the Royal Society of London* 1881; **33**:127-39.
- (2) Taylor F.W. On the art of cutting metals. *Transactions from the American Society of Metals* 1907; **28**: 31-350.
- (3) Ernst H. Physics of metal cutting, machining of metals. *Transactions from the American Society of Metals* 1938; 1-34.
- (4) Finnie I. Review of the Metal Cutting Theories of the Past Hundred Years. *Mechanical Engineering* 1956;**78**: 715-21.
- (5) Ernst H, Merchant ME. Chip Formation, Friction, and High Quality Machined Surfaces. *Trans ASME* 1941;**29**:299-328.
- (6) Lee E.H, Shaffer B.W. The Theory of Plasticity Applied to a Problem of Machining. *Journal of Applied Mechanics, Vol 18 Trans ASME* 1951; **73**:405-13.
- (7) Hill R. The Mechanics of Machining: A New Approach. *Journal of the Mechanics of Physics of Solids* 1954; **3**:47-53.
- (8) Eggleston D.M, Herzog R, Thomsen EG. Observations on the Angle Relationships in Metal Cutting. *Journal of Engineering for Industry* 1959 August; 263-79.
- (9) Reuleaux F., Über den Taylor Whiteschen Werkzeugstahl Verein sur Berforderung des Gewerbefleissen , *Sitzungsberichte* Col. 79, No 1, 1900, 179-220.
- (10) Atkins A.G. Modelling metal cutting using modern ductile fracture mechanics: quantitative explanations for some longstanding problems. *International Journal of Mechanical Sciences* 2003; **45**:373-96.
- (11) Atkins A.G. Toughness and cutting: a new way of simultaneously determining ductile fracture toughness and strength. *Engineering fracture mechanics* 2005; **72**: 849-60.
- (12) Williams J.G. Friction and plasticity effects in edge splitting and cutting fracture tests. *Journal of Materials science* 1998; **33**:5351-7.
- (13) Cotterell B, Hbaieb K, Williams J.G, Hadavinia H, Tropsa V. The root rotation in double cantilever beam and peel tests. *Mechanics of Materials* 2006; **38**:571-84.
- (14) Lau C.C, Williams J.G, Kinloch A.J. The Peeling of Flexible Laminates. *International Journal of Fracture* 1994; **66**:45-70.
- (15) Merchant M.E. Mechanics of the Metal Cutting Process. I. Orthogonal Cutting and a Type 2 Chip. *Journal of Applied Physics* 1945 May; **16**(5):267-75.
- (16) Patel Y, Williams J.G, Blackman B.R.B.K. To be published, 2008.
- (17) Kobayashi A. *Machining of Plastics*. McGraw-Hill, 1967.
- (18) Williams J.G. The Cutting of Polymers Incorporating Toughness and Adhesion Parameters; ESIS TC4 documentation for cutting protocol. 2006.
- (19) Wyeth D.J. An investigation into the mechanics of cutting using data from orthogonally cutting Nylon 66. *International Journal of Machine Tools and Manufacture* 2008; **48**:896-904.